INORGANIC CHEMISTRY FRONTIERS

RESEARCH ARTICLE

View Article Online
View Journal | View Issue

Cite this: *Inorg. Chem. Front.*, 2026, **13**, 4097

Breaking the excitation barrier: visible-light-harvesting Ir(III)–Eu(III) dyads for circularly polarized luminescence and theranostics

Zhiming Wang,[a,b] Shiwei Dong,[a,b] Chuanliang Yang,[a,b] Jinyi Chen,[a,b] Wentao Wang,*[a] Tao Li,[a,b] Guoqiang Yang *[a,b,c] and Zhong Han *[a,b]

Received 19th December 2025,
Accepted 15th March 2026

DOI: 10.1039/d5qi02548f

rsc.li/frontiers-inorganic

The application of lanthanide-based circularly polarized luminescence (CPL) probes in biological systems has long been impeded by a fundamental trade-off: the need for high-energy ultraviolet excitation to overcome the low absorptivity of f–f transitions *versus* the phototoxicity and poor tissue penetration inherent to UV irradiation. Herein, we resolve this "excitation bottleneck" by engineering a heteronuclear Ir(III)–Eu(III) dyad that functions as a highly efficient, visible-light-harvesting CPL generator. By exploiting the broad metal-to-ligand charge transfer (MLCT) absorption of a cyclometalated Ir(III) antenna, we successfully red-shift the excitation window to the benign visible region (λ_{ex} > 425 nm), extending up to ~500 nm. This sensitization strategy yields intense red Eu(III)-based emission with a substantial luminescence dissymmetry factor ($|g_{lum}|$ = 0.114) without requiring deleterious UV light. Capitalizing on this visible-light accessibility and the kinetic inertness of the rigid DO3A scaffold, we demonstrate dual-modal one- and two-photon confocal imaging in living cells. Furthermore, the dyad exhibits efficient singlet oxygen generation (Φ_Δ = 0.82), enabling photodynamic therapy. This work establishes a versatile paradigm for visible-light-driven lanthanide chiroptics, effectively bridging the gap between superior chiral photophysical properties and biocompatible excitation requirements.

Circularly polarized luminescence (CPL) originating from trivalent lanthanide (Ln^{3+}) complexes is at the forefront of photonic innovation, enabling advancements in volumetric 3D displays, quantum information processing, and enantioselective sensing.[1–6] Compared to organic CPL fluorophores,[6] lanthanide based CPL emitters offer superior spectral purity, long luminescence lifetimes (μs–ms),[7,8] and crucially, high luminescence dissymmetry factors (g_{lum}) derived from magnetic-dipole allowed f–f transitions.[1,9,10] Despite these merits, the utility of Ln(III) chiroptical materials is severely compromised by an intrinsic excitation barrier: the Laporte-forbidden nature of 4f–4f transitions results in negligible extinction coefficients (ε < 10 L mol^{-1} cm^{-1}), rendering direct excitation impractical for many applications.[11]

To overcome this transparency, conventional sensitization relies on UV-absorbing organic antennae (λ_{ex} < 400 nm).[12–14] However, high-energy UV irradiation is detrimental in biological contexts, causing background autofluorescence, limited penetration depth, and rapid phototoxicity.[15] While two-photon excitation (TPE) has been explored as an attractive workaround to circumvent UV toxicity and achieve deep-tissue penetration,[16,17] the requirement for sophisticated laser equipment limits its ubiquitous use in routine diagnostics. Consequently, developing robust Ln(III) CPL emitters that can efficiently harvest benign, one-photon visible light for standard imaging, while simultaneously possessing high TPE capabilities for deep-tissue theranostics, remains a highly desirable, yet unmet, challenge in the field.

Herein, we introduce a strategy to surmount this barrier by employing a cyclometalated iridium(III) complex as visible-light-harvesting antenna.[18,19] Unlike organic dyes, Ir(III) chromophores possess broad, intense metal-to-ligand charge transfer (MLCT) absorptions in the visible spectrum and long-lived triplet states accessible *via* strong spin–orbit coupling.[20–22] By integrating an Ir(III) donor with a chiral Eu(III) acceptor,[18,23–25] we construct heteronuclear dyads capable of efficient visible-light sensitization (λ_{ex} > 425 nm) *via* d–f energy transfer mechanism. This approach successfully translates the visible absorption of Ir(III) into the circularly polarized emis-

[a]*Postgraduate training base Alliance of Wenzhou Medical University, Wenzhou 325035, China. E-mail: wangwentao@wiucas.ac.cn, litao@ucas.ac.cn, gqyang@iccas.ac.cn, z_han@wiucas.ac.cn*
[b]*Wenzhou Institute, University of Chinese Academy of Sciences, Wenzhou, Zhejiang 325000, China*
[c]*Key Laboratory of Photochemistry, Institute of Chemistry, Chinese Academy of Sciences, Beijing 100190, China*

sion of Eu(III), establishing a versatile paradigm for low-energy excited Ln(III) based chiroptical materials.

The heteronuclear Ir(III)–Eu(III) CPL emitters were constructed *via* a "complex-as-ligand" strategy to ensure precise stoichiometric control and rigid stereochemical definition (Fig. 1). The Eu(III) chiral DO3A complexes were synthesized and fully characterized (see SI). Subsequent coordination with Ir(III) moiety afforded the target visible-light-excited heteronuclear Ir(III)–Eu(III) CPL complexes in moderate yields. The formation of the binuclear complexes was confirmed by high resolution mass spectroscopy and HPLC (SI).

With the structural integrity confirmed, photophysical properties to validate the excitation barrier breakthrough were investigated and were summarized in Table S1. As shown in Fig. 2a and S1, the absorption spectra of the complexes were dominated by broad, intense bands in the visible region of 380–500 nm, assigned to spin-allowed ^{1}MLCT and spin-forbidden ^{3}MLCT transitions localized on the Ir(III) antenna. This stands in stark contrast to the negligible extinction coefficient of the Eu(III) precursor in this range.[12] Upon excitation into the Ir(III)-based MLCT band at 425 nm, the complexes exhibited the characteristic, sharp emission lines of the Eu(III) ion, dominated by the hypersensitive $^{5}D_0 \rightarrow {}^{7}F_2$ electric dipole transition at 616 nm

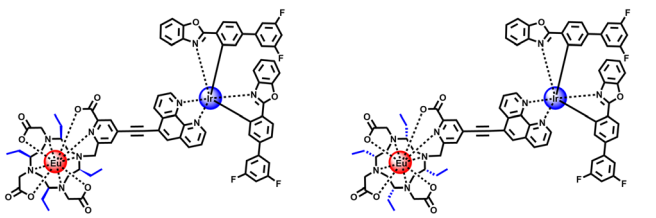

Fig. 1 Chemical structures of the CPL complexes (**S–Ir–Eu** and **R–Ir–Eu**).

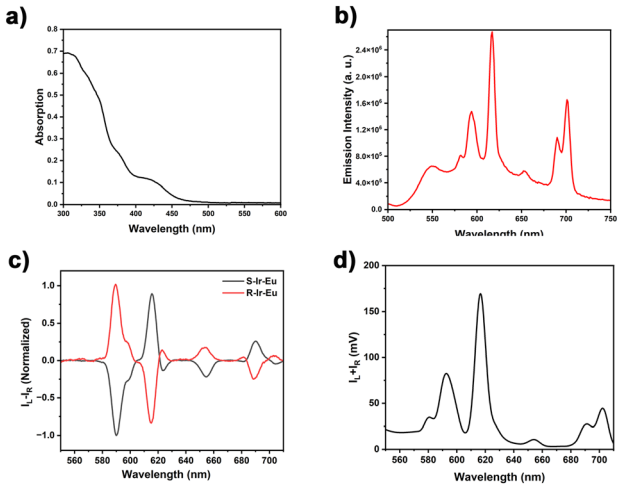

Fig. 2 UV-Vis absorption (a, 10 μM) and emission spectra (b, 10 μM, λ_{ex} = 425 nm) of **S–Ir–Eu** in HEPES buffer containing 1% DMSO (pH 7.40), and CPL spectra (c) with total luminescence (d) in MeOH (λ_{ex} = 425 nm).

(Fig. 2b). The excitation spectrum monitored at 616 nm overlaps perfectly with the Ir(III) absorption profile, providing conclusive evidence that the Eu(III) luminescence is exclusively sensitized by the visible-light-harvesting Ir(III) antenna (Fig. S1).

Crucially, the structural design plays a vital role in maintaining this efficiency. Although the Ir(III) antenna introduces high-frequency C–H oscillators that could potentially quench the Eu(III) emission, the rigid ethynyl-pyridine linker effectively mitigates this by enforcing a critical spatial separation. This design minimizes multiphonon relaxation, allowing the efficient energy transfer to dominate over nonradiative deactivation. Furthermore, the macrocyclic DO3A scaffold effectively shields the Eu(III) center from water quenching ($q \approx 0$, Table S1), ensuring robust sensitization. Moreover, two-photon excitation was also achieved for the two enantiomers *via* irradiating with the complexes at different excitation wavelength ranging from 750 nm to 900 nm (Fig. S3).

To further elucidate the energy transfer (EnT) mechanism, the phosphorescence decay kinetics were investigated using Time-Correlated Single Photon Counting (TCSPC). The Gd(III) analogue (**S–Ir–Gd**, Fig. S4) was synthesized as an energetically equivalent reference to determine the intrinsic lifetime of the Ir(III) donor. While **S–Ir–Gd** exhibited a long-lived emission (τ = 1.02 μs), the lifetimes of the Ir(III) moiety in the dyads were drastically quenched to 50 ns (**S–Ir–Eu**) and 53 ns (**R–Ir–Eu**) upon coordination with the Eu(III) center. Based on these values, the EnT efficiencies (η_{EnT}) were calculated to be 95.1% and 94.8%, respectively, with rate constants (k_{EnT}) of approximately 1.90×10^{7} s^{-1} and 1.79×10^{7} s^{-1}. Given the negligible extinction coefficient of the Laporte-forbidden f–f transitions of Eu(III), which precludes efficient Förster transfer, we attribute this rapid and efficient sensitization to a Dexter-type electron exchange mechanism facilitated by the strong electronic coupling of the conjugated ethynyl-pyridine linker.

To correlate the ground-state and excited-state chiroptical properties, circular dichroism (CD) spectra were recorded in HEPES buffer (Fig. S5). The spectra reveal a distinct dichotomy: while the UV region (<400 nm) exhibits mirror-image Cotton effects ($g_{abs} \approx 5.6 \times 10^{-5}$) confirming the structural enantiopurity of the scaffold, the visible MLCT region is chiroptically silent. Specifically, at the excitation wavelength (425 nm), the absorption dissymmetry factor (g_{abs}) is negligible (2.6×10^{-6}), indicating that the Ir(III) antenna absorbs light as an essentially optically inactive entity. This stark contrast with the giant g_{lum} highlights a remarkable chiral amplification mechanism. It confirms that the system functions by converting a non-stereoselective photon input into a highly polarized luminescence output *via* efficient energy transfer to the chiral Eu(III) core, effectively ruling out absorption-induced polarization artifacts.

With efficient visible-light sensitization established, the chiroptical properties of the heteronuclear CPL complexes were investigated. Upon excitation at 425 nm, the complexes exhibit distinct circularly polarized luminescence signatures, with the enantiomers displaying perfect mirror-image spectra (Fig. 2c, d and S6). Notably, the CPL profile is dominated by the magnetic dipole-allowed $^{5}D_0 \rightarrow {}^{7}F_1$ transition (ΔJ = 1) at

approximately 590 nm. Although the hypersensitive electric dipole-allowed $^5D_0 \rightarrow {}^7F_2$ transition (~616 nm) dictates the total emission intensity, its contribution to the differential emission (ΔI, $I_L - I_R$) is attenuated by the negligible magnetic transition dipole moment characteristic of $\Delta J = 2$ transitions. Consequently, the luminescence dissymmetry factor is significantly maximized within the $\Delta J = 1$ manifold, yielding a $|g_{lum}|$ value of 0.114 (590 nm) compared to 0.047 for the $\Delta J = 2$ band (616 nm). The persistence of these intense, structured signals confirms that the rigid DO3A-Ir(III) architecture effectively suppresses excited-state racemization, preserving a static chiral environment around the Eu(III) center throughout the tens of microseconds luminescence decay. To further probe the electronic nature of these transitions, magnetic CPL (MCPL) measurements were conducted. The dissymmetry factor of the $^5D_0 \rightarrow {}^7F_1$ transition exhibited a distinct dependence on the external magnetic field strength; for **R–Ir–Eu**, the $|g_{lum}|$ value was enhanced by 29.8%, increasing from 0.114 at 0 T to 0.148 at 1.6 T (Fig. S7). This field-induced amplification underscores the dominant magnetic dipole character of the transition and confirms the sensitivity of the CPL complex to external magnetic perturbations.[12,26] Moreover, quantitative analysis reveals that the dyads exhibit impressive CPL brightness $(B_{CPL})^1$ values of 8.9 M^{-1} cm^{-1} (**R–Ir–Eu**) and 9.1 M^{-1} cm^{-1} (**S–Ir–Eu**). Such high values are particularly desirable for practical applications in 3D displays and CPL-based bioimaging, where both signal intensity and chiral discrimination capability are critical. This superior performance is superior to many reported organic CPL materials, confirming the value of the antenna-sensitized lanthanide architecture.

To function effectively as a chiroptical probe in biological systems, the complex must satisfy stringent criteria regarding aqueous solubility, emissive efficiency, and high luminescence dissymmetry factors.[12] We initially investigated the solvent dependence of the CPL signature, conducting measurements in 0.1 M HEPES, MeOH, THF, DMSO, and DCM. While the spectral topology of **S–Ir–Eu** remained consistent across all media, the magnitude of the dissymmetry factor exhibited sensitivity to the local environment, ranging from −0.051 in aqueous HEPES to −0.114 in MeOH (Fig. 3a).

To elucidate the origin of this variation, luminescence lifetime measurements using the Horrocks and Parker methods yielded a hydration number (q) of approximately zero (Table S1). This confirms a saturated 9-coordinate environment that effectively precludes direct solvent binding. Consequently, the observed solvent dependence of g_{lum} is attributed to outer-sphere perturbations.[27] We propose that hydrogen bonding interactions between the solvent and the ligand backbone induce subtle geometric distortions in the coordination polyhedron. Given the hypersensitivity of Eu(III) transitions to symmetry, these solvation-induced conformational changes are sufficient to significantly modulate the chiroptical output.

Crucially, while the chiroptical output responds to the solvent environment, the chemical stability of the scaffold remains robust. pH titrations revealed negligible spectral deviation across a broad window (pH 4–9), confirming that the heteronuclear architecture resists acid-promoted decomplexation and maintains its coordination geometry even under physiologically extreme conditions (Fig. 3b).

Beyond chemical robustness, luminescent imaging requires probes with high resistance to photobleaching and metabolic degradation. **S–Ir–Eu** demonstrated excellent photostability under continuous irradiation, showing no evidence of decomposition (Fig. S8). To simulate complex physiological environments, the stability was further challenged against a competitive "anion cocktail" (containing 0.9 mM HPO_4^{2-}, 100 mM Cl^-, 2.3 mM lactate, 0.13 mM citrate and 15 mM HCO_3^-),[28] essential amino acids (Glu, His, Thr) and human serum albumin (HSA). The complex exhibited invariant luminescence intensity and preserved spectral splitting patterns under these conditions, indicating inertness against biophysical complicated environment (Fig. S9). Furthermore, incubation in fetal bovine serum (FBS) for 25 h resulted in negligible loss of phosphorescence intensity (Fig. S10), underscoring the suitability of **S–Ir–Eu** for prolonged biological studies.

Leveraging the efficient visible-light sensitization of the Ir(III) antenna, we evaluated the intracellular performance of the heteronuclear dyad. HeLa cells incubated with **S–Ir–Eu** and **R–Ir–Eu** displayed intense luminescence under both one-photon (λ_{ex} = 405 nm) and two-photon (λ_{ex} = 850 nm) excitation (Fig. 4a & S12). The detection of Eu(III) emission confirms successful cellular internalization and the preservation of the Ir → Eu energy transfer pathway within the cytosol. Concurrently,

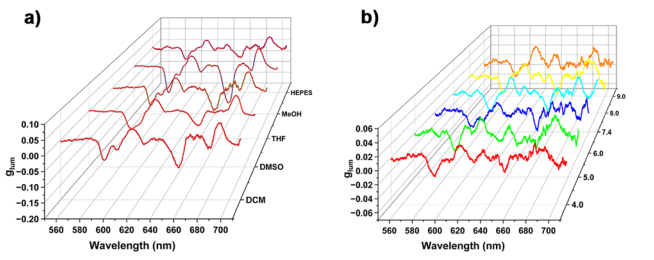

Fig. 3 g_{lum} spectra of **S–Ir–Eu** in different solvent (a) and under different pH (b), λ_{ex} = 425 nm.

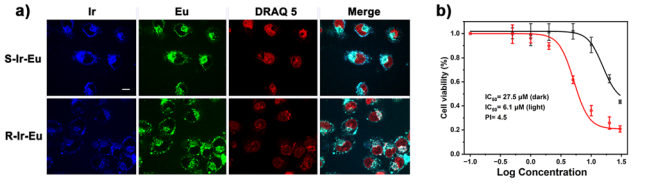

Fig. 4 (a) Confocal images of HeLa cells co-stained by **S–Ir–Eu** or **R–Ir–Eu** (20 μM in DMEM medium with 1% DMSO, λ_{ex} = 405 nm, 12 h) and DRAQ 5 (a, 1 μM, λ_{ex} = 640 nm, 10 min). Scale bar: 10 μm. Bandpaths: Ir (500–550 nm), Eu (570–620 nm), DRAQ 5 (663–738 nm); (b) cytotoxicities of **S–Ir–Eu** against HeLa cell line determined after 24 h of incubation under dark conditions with (red) or without (black) photoirradiation (450 nm, 30 J cm^{-2}, 60 s) at the 4th hour of incubation.

the complex exhibits a substantial singlet oxygen generation quantum yield (Φ_Δ = 0.82), prompting an evaluation of its photodynamic efficacy *via* standard CCK-8 assays. While the complex displayed low dark cytotoxicity (IC_{50} = 27.5 μM), photo-irradiation (450 nm, 60 s, 30 J cm^{-2}) induced a marked therapeutic effect, lowering the IC_{50} to ~6.1 μM. This significant light-triggered toxicity yields a phototherapeutic index (PI) exceeding 4.5, establishing **S–Ir–Eu** as a promising candidate for dual-functional theranostics.

Conclusions

In conclusion, we have successfully engineered a series of nine-coordinated chiral DO3A-Eu(III) enantiomers, utilizing a cyclometalated iridium(III) unit as a robust visible-light-harvesting antenna. This heterometallic design effectively circumvents the UV-excitation limitations of traditional organic-lanthanide CPL chelates, extending the operational excitation window up to ~500 nm while preserving a substantial luminescence dissymmetry factor ($|g_{lum}|$ = 0.114). Crucially, by taking advantage of this red-shifted excitation capability of the antenna, we realized visible-light-driven confocal luminescence imaging and effective photodynamic therapy (PDT) in living systems. This synergistic Ir(III)–Eu(III) strategy successfully resolves the historical trade-off between visible light excitation efficiency and chiroptical performance, providing a robust scaffold for advanced bio-photonic CPL applications. Ongoing efforts are currently directed toward optimizing the d–f energy transfer kinetics and employing CPL laser scanning microscopy as a tool to interrogate dynamic chiral molecular interactions within the cellular environment.

Conflicts of interest

There are no conflicts to declare.

Data availability

All data generated or analyzed during this study are included in this published article and its supplementary information (SI). Supplementary information is available. See DOI: **https://doi.org/10.1039/d5qi02548f**.

Acknowledgements

The authors wish to thank financial supports from National Natural Science Foundation of China (No. 22201055), Natural Science Foundation of Zhejiang Province (No. LQ23B010002) and start-up grant from Wenzhou Institute, University of Chinese Academy of Sciences (No. WIUCAS2023001).

References

1 C. A. Guido, F. Zinna and G. Pescitelli, Quantum Chemistry Calculations of Circularly Polarized Luminescence (CPL): From Spectral Modeling to Molecular Design, *Chem. Rev.*, 2025, **125**, 10492–10656.
2 L. Xu, X. Wang, W. Wang, M. Sun, W. J. Choi, J.-Y. Kim, C. Hao, S. Li, A. Qu, M. Lu, X. Wu, F. M. Colombari, W. R. Gomes, A. L. Blanco, A. F. De Moura, X. Guo, H. Kuang, N. A. Kotov and C. Xu, Enantiomer-dependent immunological response to chiral nanoparticles, *Nature*, 2022, **601**, 366–373.
3 X. Yang, X. Gao, Y.-X. Zheng, H. Kuang, C.-F. Chen, M. Liu, P. Duan and Z. Tang, Recent Progress of Circularly Polarized Luminescence Materials from Chinese Perspectives, *CCS Chem.*, 2023, 1–34.
4 Y. Zhang, S. Yu, B. Han, Y. Zhou, X. Zhang, X. Gao and Z. Tang, Circularly polarized luminescence in chiral materials, *Matter*, 2022, **5**, 837–875.
5 J. Zhao, S. Shi, X. Zhang, D. Liu, F. Song, Y. Cheng and F. Li, Circularly polarized luminescence pyrene materials: From design to applications, *Coord. Chem. Rev.*, 2026, **548**, 217173.
6 Z.-L. Gong, X. Zhu, Z. Zhou, S.-W. Zhang, D. Yang, B. Zhao, Y.-P. Zhang, J. Deng, Y. Cheng, Y.-X. Zheng, S.-Q. Zang, H. Kuang, P. Duan, M. Yuan, C.-F. Chen, Y. S. Zhao, Y.-W. Zhong, B. Z. Tang and M. Liu, Frontiers in circularly polarized luminescence: molecular design, self-assembly, nanomaterials, and applications, *Sci. China: Chem.*, 2021, **64**, 2060–2104.
7 D. Parker, J. D. Fradgley and K.-L. Wong, The design of responsive luminescent lanthanide probes and sensors, *Chem. Soc. Rev.*, 2021, **50**, 8193–8213.
8 Y. Chen, Y. Bai, Z. Han, W. He and Z. Guo, Photoluminescence imaging of Zn^{2+} in living systems, *Chem. Soc. Rev.*, 2015, **44**, 4517–4546.
9 M. Tsurui, R. Takizawa, Y. Kitagawa, M. Wang, M. Kobayashi, T. Taketsugu and Y. Hasegawa, Chiral Tetrakis Eu(III) Complexes with Ammonium Cations for Improved Circularly Polarized Luminescence, *Angew. Chem., Int. Ed.*, 2024, **63**, e202405584.
10 J. A. Adewuyi and G. Ung, High Quantum Yields from Perfluorinated Binolate Erbium Complexes and Their Circularly Polarized Luminescence, *J. Am. Chem. Soc.*, 2024, **146**, 7097–7104.
11 R. Carr, N. H. Evans and D. Parker, Lanthanide complexes as chiral probes exploiting circularly polarized luminescence, *Chem. Soc. Rev.*, 2012, **41**, 7673.
12 J. Zhang, L. Dai, A. M. Webster, W. T. K. Chan, L. E. Mackenzie, R. Pal, S. L. Cobb and G. Law, Unusual Magnetic Field Responsive Circularly Polarized Luminescence Probes with Highly Emissive Chiral Europium(III) Complexes, *Angew. Chem., Int. Ed.*, 2021, **60**, 1004–1010.
13 L. Dai, W.-S. Lo, I. D. Coates, R. Pal and G.-L. Law, New Class of Bright and Highly Stable Chiral Cyclen Europium

Complexes for Circularly Polarized Luminescence Applications, *Inorg. Chem.*, 2016, **55**, 9065–9070.

14 L. Dai, C. M. Jones, W. T. K. Chan, T. A. Pham, X. Ling, E. M. Gale, N. J. Rotile, W. C.-S. Tai, C. J. Anderson, P. Caravan and G.-L. Law, Chiral DOTA chelators as an improved platform for biomedical imaging and therapy applications, *Nat. Commun.*, 2018, **9**, 857.

15 O. G. Willis, F. Petri, D. F. De Rosa, A. Mandoli, R. Pal, F. Zinna and L. Di Bari, Two-Photon Circularly Polarized Luminescence of Chiral Eu Complexes, *J. Am. Chem. Soc.*, 2023, **145**, 25170–25176.

16 P. Stachelek, L. MacKenzie, D. Parker and R. Pal, Circularly polarised luminescence laser scanning confocal microscopy to study live cell chiral molecular interactions, *Nat. Commun.*, 2022, **13**, 553.

17 L. Wu, J. Liu, P. Li, B. Tang and T. D. James, Two-photon small-molecule fluorescence-based agents for sensing, imaging, and therapy within biological systems, *Chem. Soc. Rev.*, 2021, **50**, 702–734.

18 K. Xu, X. Xie and L.-M. Zheng, Iridium-lanthanide complexes: Structures, properties and applications, *Coord. Chem. Rev.*, 2022, **456**, 214367.

19 Z. Wang, L. Wang, S. Dong, C. Yang, J. Chen, W. Wang, G. Yang and Z. Han, Rational Design of Rigid Chiral Ir(III)–Eu(III) Dyads: Intense Circularly Polarized Luminescence via Visible-Light Sensitization, *Inorg. Chem.*, 2026, **65**, 3209–3214.

20 Z. Han, Y. Chen, Y. Wang, X. Shi, H. Yuan, Y. Bai, Z. Chen, H. Fang, W. He and Z. Guo, Photoinduced synergistic cytotoxicity towards cancer cells via Ru(II) complexes, *Dalton Trans.*, 2020, **49**, 13954–13957.

21 Z. Han, Y. Wang, Y. Chen, H. Fang, H. Yuan, X. Shi, B. Yang, Z. Chen, W. He and Z. Guo, A novel luminescent Ir (III) complex for dual mode imaging: synergistic response to hypoxia and acidity of the tumor microenvironment, *Chem. Commun.*, 2020, **56**, 8055–8058.

22 H. Yuan, Z. Han, Y. Chen, F. Qi, H. Fang, Z. Guo, S. Zhang and W. He, Ferroptosis Photoinduced by New Cyclometalated Iridium(III) Complexes and Its Synergism with Apoptosis in Tumor Cell Inhibition, *Angew. Chem., Int. Ed.*, 2021, **60**, 8174–8181.

23 L.-J. Xu, G.-T. Xu and Z.-N. Chen, Recent advances in lanthanide luminescence with metal-organic chromophores as sensitizers, *Coord. Chem. Rev.*, 2014, **273–274**, 47–62.

24 D. Sykes, I. S. Tidmarsh, A. Barbieri, I. V. Sazanovich, J. A. Weinstein and M. D. Ward, d → f Energy Transfer in a Series of Ir III/Eu III Dyads: Energy-Transfer Mechanisms and White-Light Emission, *Inorg. Chem.*, 2011, **50**, 11323–11339.

25 E. Baggaley, D.-K. Cao, D. Sykes, S. W. Botchway, J. A. Weinstein and M. D. Ward, Combined Two-Photon Excitation and d→f Energy Transfer in a Water-Soluble Ir III/Eu III Dyad: Two Luminescence Components from One Molecule for Cellular Imaging, *Chem. – Eur. J.*, 2014, 8898–8903.

26 D. A. Gálico and M. Murugesu, Magnetic Circularly Polarized Luminescence with Heterometallic Molecular Cluster–Aggregates, *Adv. Opt. Mater.*, 2024, **12**, 2401064.

27 J.-R. Jiménez, B. Doistau, C. M. Cruz, C. Besnard, J. M. Cuerva, A. G. Campaña and C. Piguet, Chiral Molecular Ruby $[Cr(dqp)_2]^{3+}$ with Long-Lived Circularly Polarized Luminescence, *J. Am. Chem. Soc.*, 2019, **141**, 13244–13252.

28 S. J. Butler and D. Parker, Anion binding in water at lanthanide centres: from structure and selectivity to signalling and sensing, *Chem. Soc. Rev.*, 2013, **42**, 1652–1666.